Fe$_3$S$_4$/Fe$_7$S$_8$-promoted degradation of phenol via heterogeneous, catalytic H$_2$O$_2$ scission mediated by S-modified surface Fe^{2+} species

Yun Jeong Choe[a], Ji Young Byun[a,b], Sang Hoon Kim[a,b,*], Jongsik Kim[a,*]

[a] Materials Architecting Research Center, Korea Institute of Science and Technology, 5, Hwarang-ro 14-gil, Seongbuk-gu, Seoul, 02792, Republic of Korea
[b] Department of Nanomaterials Science and Engineering, University of Science and Technology, 217, Gajeong-ro, Yuseong-gu, Daejeon, 34113, Republic of Korea

ABSTRACT

Enhancing ·OH productivity via heterogeneous, catalytic H$_2$O$_2$ activation is a long-standing conundrum in H$_2$O purification and thus requires the renovation of conventional reaction systems. The initial step in realizing advanced H$_2$O$_2$ decomposition via heterogeneous catalytic manner is the exploration of the solid capable of efficiently cleaving O─O bond inherent to H$_2$O$_2$ and minimizing the loss of catalytic species during vigorous reaction dynamics. While using phenol as a model compound for recalcitrants, this paper highlights the use of Fe$_3$S$_4$/Fe$_7$S$_8$ as a catalyst to enhance ·OH productivity and thus promote phenol degradation via electro-Fenton reaction over conventional Fe$_2$O$_3$, Fe$_3$O$_4$, and other sulfide analogue (FeS$_2$). Materials' characterizations and kinetic interpretation of reaction runs under controlled environments served to substantiate the benefits which were provided by Fe$_3$S$_4$/Fe$_7$S$_8$ during the reaction. Fe$_3$S$_4$/Fe$_7$S$_8$ incorporated greater amount of S-modified, surface-exposed Fe^{2+} sites to cleave H$_2$O$_2$ than FeS$_2$. This improved catalytic consequence of Fe$_3$S$_4$/Fe$_7$S$_8$ (i.e., phenol conversion and initial reaction rate), as also evidenced by control runs detailing H$_2$O$_2$ decomposition in conjunction with *tert*-butyl alcohol-driven ·OH scavenging. Filtration control runs as well as recycle runs were also used to verify that Fe$_3$S$_4$/Fe$_7$S$_8$ could heterogeneously catalyze H$_2$O$_2$ scission under the mild, adequate reaction environments, which were realized by the use of low electrical powers and the catalyst immobilized on a cathode.

1. Introduction

Discovery of a solid, which is highly active to dissociate H$_2$O$_2$ for ·OH evolution via heterogeneous catalysis, is particularly conducive to the efficient/sustainable decomposition of recalcitrant, non-biodegradable chemicals in the wastewater stream [1–3]. Advanced oxidation process (AOP) is deemed as a promising means 1) to mitigate increasing demands on H$_2$O purification and 2) to satisfy corresponding regulations with substantial stringency to-date [4,5]. This liquid-phase catalytic process is featured by oxidants which are initially added to the process (e.g., O$_2$, O$_3$, and H$_2$O$_2$) and subsequently dissociated via photo- or homogeneous-catalysis to form various radicals (e.g., ·O^{2-}, ·OOH, and ·OH) [1–5]. These are electrophiles and thus exhibit appreciable activity to fragment refractory petroleum-based pollutants via a series of radicals-propagated reactions to finally produce H$_2$O and CO$_2$ (Fig. 1(a)). Among various oxidants, H$_2$O$_2$ was reported to outperform the others due to its strongest standard oxidation potential (i.e., 2.8 eV for ·OH; 1.8 eV for ·OOH; −2.4 eV for ·O^{2-}) [6–8].

Among various AOPs, Fenton reaction is known as an advanced, cheap, and highly efficient way to remedy H$_2$O contamination [1–8]. Its conventional version utilizes Fe salts-ionized, homogeneous Fe^{2+} species as H$_2$O$_2$ scissors to evolve −OH and ·OH oxidants, while involving the oxidation of Fe^{2+} to Fe^{3+} (Fig. 1(b)) [1–8]. This shows ·OH-driven outstanding oxidative capacity to degrade contaminants, yet, also requires its operation at optimum pH value of ∼3 to minimize the rapid accumulation of Fe(OH)$_3$ [1–8]. In addition to difficulties in recovering Fe^{2+} species from effluents, the resulting precipitate is detrimental to retain Fe^{2+}/Fe^{3+} redox-cycle during the reaction, thereby oftentimes terminating the reaction while leaving the contaminants un-oxidized [1–8].

This issue suggested the use of Fe-bearing materials (e.g., Fe$_2$O$_3$, Fe$_3$O$_4$, or metallic Fe) as Fe^{2+} shuttles that were expected to deliver a far greater amount of dissolved Fe^{2+} species than Fe salts employed during conventional Fenton reaction (denoted as Fenton-like reaction) [9–11]. The Fenton-like reaction, however, turned out to primarily catalyze ·OH evolution via Fe^{3+}-H$_2$O$_2$ interactions, leading to sluggish ·OH production rates compared to conventional counterpart [10,12,13]. To circumvent drawbacks of conventional Fenton and Fenton-like reactions, electro-Fenton reaction was suggested as an alternative [2,5,8,9]. This novel reaction initially electrolyzed H$_2$O to
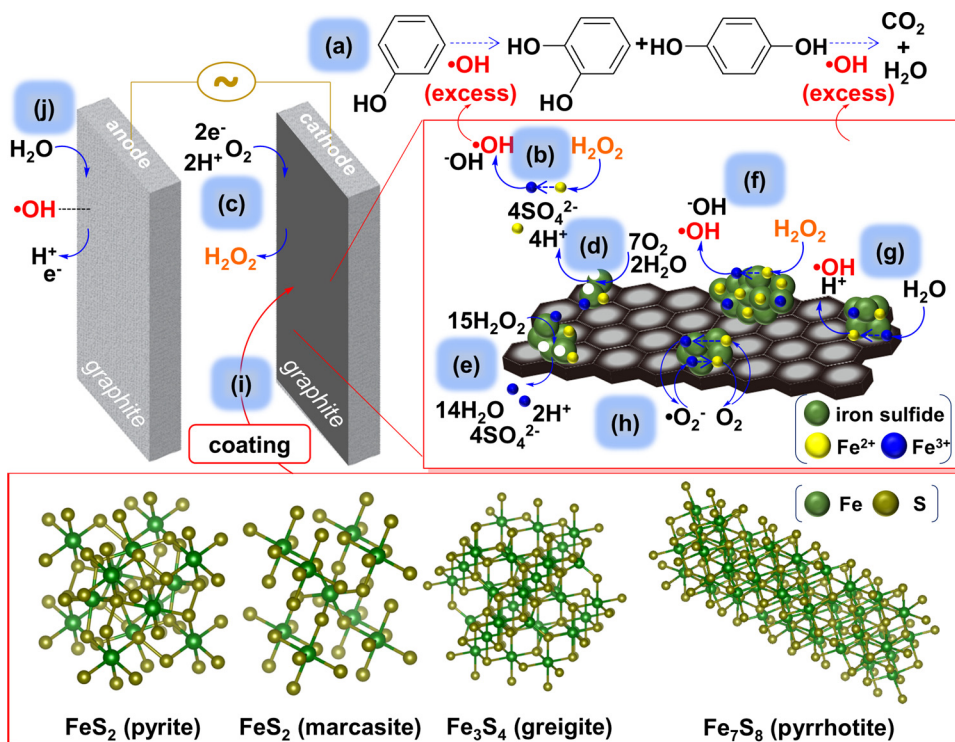
Fig. 1. Schematic representation of electro-Fenton reaction system to degrade phenol: reaction pathway of ·OH-assisted phenol decomposition (a), reactions on anode (j)/cathode (c) coated with various Fe sulfides (i), and a series of reactions accounting for Fe^{2+}/Fe^{3+}-mediated ·OH evolution via homogeneous (b, d, and e) and heterogeneous manners (f, g, and h). In (a), chemical stoichiometry was omitted for simplicity.

generate H^+, O_2, electron (e^-), etc. and provided virtually infinite amount of H_2O_2 via continuous O_2 reduction on a cathode (Fig. 1(c)) [2,5,8,9]. In addition, sufficient electrons which were formed during electro-Fenton reaction could help reduce Fe^{3+} to Fe^{2+} and therefore eliminated the need of separate, homogeneous Fe^{2+} providers for continuous ·OH generation [2,5,8,9].

To achieve greater ·OH production activities, the type of Fe-bearing materials was altered to Fe sulfides. Indeed, Fe sulfides' surface comprises of an interesting class of catalytic functional groups ranging from Lewis basic ≡SH to e^--abundant, reduced Fe and S species [8,14,15]. In particular, Fe surface species on pyrite (FeS_2) and its S-modified crystal structure could render the surface to favorably interact with O_2 and H_2O_2 and boost the formation of homogenous Fe^{2+} and Fe^{3+} species during (electro-) Fenton reactions [13,16–21]. Specifically, resulting Fe^{2+} and Fe^{3+} species subsequently facilitated the generation of ·OH and additional homogeneous Fe^{2+} species through the interaction with pyrite surface in the presence of H_2O, respectively [13,16,17]. Of note, Brillas and co-workers suggested these promotional effects were more pronounced under specific electro-Fenton reaction environments, where pyrite was suspended into H_2O, leading to pH value of ∼3 in the presence of O_2 bubbling at large electrical powers (i.e., 0.4–5.5 W) [22]. While it should not be denied that aforementioned findings were quite impressive and interesting, the reaction condition was still severe. This resulted in ·OH production performance to be mainly directed by homogeneous (leached) Fe^{2+} species (e.g., Fig. 1(b), (d), and (e)) rather than surface-exposed (unleached) Fe^{2+} species (e.g., Fig. 1(f)–(h)) [22]. Of additional note, D. Wu and co-workers proposed the pyrite could generate ·OH via heterogeneous catalysis under alkaline condition. This was realized through the addition of homogeneous S^{2-} species during the reaction (i.e., Na_2S), which aided in reconstructing FeS_n surfaces that were active to yield ·OH [23]. Multiple previous Fenton studies also corroborated heterogeneous catalytic nature of pyrite or S-doped Fe oxide to efficiently produce ·OH via peculiar Fe-S molecular orbital or enhanced e^- transfer between Fe^{2+} and radicals [24,25]. The catalytic ·OH production elaborated in these studies, however, also resulted from multiple H_2O_2 scission pathways, most of which followed the leached Fe^{2+} species-mediated homogeneous catalysis. To proceed

catalytic H_2O_2 scission in sustainable and economical manners, it is highly desired to maximize the portion of heterogeneous catalysis when cleaving H_2O_2 species. We thus set our 1st hypothesis that without adding S^{2-} source or pH-adjusting agents, Fe sulfides can catalyze ·OH evolution on unleached Fe^{2+} species via heterogeneous catalysis under specific electro-Fenton conditions which remain veiled so far.

In addition, our 2nd hypothesis upon structural inspection of Fe sulfides was constructed such that Fe_3S_4/Fe_7S_8 can outperform FeS_2 (pyrite and marcasite) to further enhance ·OH production-directed decomposition performance of pollutants. Specifically, greigite (Fe_3S_4) was used in this study based on the structural similarity between Fe_3O_4 and Fe_3S_4 [26,27]. Inverse spinel Fe_3O_4 was reported to play more proper role as Fe^{2+} shuttle during Fenton-like reaction than Fe_2O_3 because of more abundant Fe^{2+} species incorporated into Fe_3O_4 [28]. Hence, Fe_3S_4 iso-structural to Fe_3O_4 except the substitution of O to S was anticipated to enhance ·OH evolution than FeS_2 under adequate conditions, in which heterogeneous catalytic H_2O_2 scissions were predominant. Pyrrhotite (Fe_7S_8) also attempted to be synthesized because this includes coordinately-unsaturated (open) Fe vacancies in conjunction with longer Fe-S bond length (c.a. ∼2.5 Å) than that of pyrite (c.a. ∼2.3 Å), as clarified in crystallographic analyses on Fe_7S_8 [8,29]. In comparison with NaCl-type pyrite with rigid, dense crystal structure and no such open Fe^{2+} sites, pyrrhotite was thus expected to provide greater accessibility of H_2O_2 to surface-terminated Fe^{2+} species and facilitate heterogeneous, catalytic ·OH formation.

Herein, we demonstrated our two major hypotheses, which was synopsized as heterogeneous catalysed, particularly promoted H_2O_2 scission performance on Fe_3S_4/Fe_7S_8 under H_2O electrolysis. We performed reaction runs using various Fe-bearing materials as catalysts (i.e., Fe_2O_3, Fe_3O_4, FeS_2, and Fe_3S_4/Fe_7S_8). We also chose phenol as a model compound for electro-Fenton reactions because of its ubiquitous structure comprising as a backbone of various organic contaminants (i.e., halogenated polycyclic aromatics) [30,31]. In addition to a battery of characterizations, reaction performance such as initial reaction rates as well as phenol conversions was assessed and served to compare ·OH productivity and heterogeneous catalytic nature of Fe sulfides under controlled reaction environments.

2. Material and methods

2.1. Chemicals

Chemicals were purchased from vendors and used without further purifications: $FeSO_4·7H_2O$ (Sigma-Aldrich, ≥99.0%), L-cysteine ($C_3H_7NO_2S$, JUNSEI), $Na_2S_2O_3·5H_2O$ (Sigma-Aldrich, ≥99.0%), S (Alfa-Aesar, ~325 mesh, 99.5 %), CS_2 (DAEJUNG, 99%), C_6H_5OH (DAEJUNG, 99%), CH_3OH (Sigma-Aldrich, 99.8% or DAEJUNG for HPLC, 99.9%), C_2H_5OH (DAEJUNG, 94.5%), Na_2SO_4 (Sigma-Aldrich, ≥99.0%), poly(acrylic acid) solution (($C_3H_4O_2$)$_n$, Sigma-Aldrich, M_w ~10^6, 35 wt. % in H_2O), Celite® 545 (YAKURI PURE), CH_3COCH_3 (DAEJUNG, 99.8%), $NH_2OH·HCl$ (Sigma-Aldrich, ≥99.0%), CH_3COONa (Sigma-Aldrich, ≥99.0%), 1,10-phenanthroline ($C_{12}H_8N_2$, Sigma-Aldrich, ≥99%), Neocuproine ($C_{14}H_{12}N_2$, Sigma-Aldrich, ≥98%), $CuSO_4·5H_2O$ (Sigma-Aldrich, ≥98.0%), phosphate buffer (SAMCHUN, pH7.2), $(NH_4)_2Fe(SO_4)_2·6H_2O$ (Sigma-Aldrich, 99%), H_2O_2 (Sigma-Aldrich, 29.0–32.0 wt. %, H_2O_2 basis), Fe_2O_3 (DAEJUNG, 93%), and Fe_3O_4 (Sigma-Aldrich, 95%).

2.2. Characterizations

Texture property of catalysts was assessed via N_2 physisorption at 77 K using ASAP 2010 (Micromeritics). Prior to analysis, the catalyst was thoroughly degassed at 150 °C for 2 hours under vacuum (~4×10^{-9} mmHg). Brunauer-Emmett-Teller (BET) surface area of catalysts was evaluated using the volume of N_2 physisorbed onto the catalyst's surface under partial pressure range (P/P_0) of 0.05–0.3. Pore volume of catalysts was evaluated via Barrett–Joyner–Halenda (BJH) method with the assumption that all pores are cylinder-shaped nanopores. X-ray diffraction (XRD) pattern of catalysts was obtained using D8 Advance (Bruker) with a scan speed of 2 s per step, a step size of 0.02° per step, and 2 theta range of 20–80° via monochromatic Cu Kα radiation (λ = 1.54 Å). High resolution transmission electron microscope (HRTEM) image and selected area electron diffraction (SAED) pattern of catalysts were attained using FEI (Titan 80–300™) at 300 keV. Prior to analysis, the catalyst was suspended in acetone, subjected to the sonication for 5 min, dropped onto a holey carbon film grid, and then dried at 40 C °under vacuum of ~2×10^{-7} torr for 5 min. CO-pulsed chemisorption analysis for catalysts was conducted using AutoChem II (Micromeritics) at 40 °C. Prior to analysis, catalyst's surface was purged at 200 °C under a He atmosphere for 3 h. X-ray photoelectron (XP) spectroscopy analysis for catalysts was performed using PHI 5000 VersaProbe post cleaning the surface of the catalyst deposited on a carbon tape under ultra-high vacuum (~2×10^{-7} Pa). Adventitious carbon located at binding energy of 284.6 eV was employed as a reference for the observation of the catalyst's surface character. Relative abundance of Fe and S species present on (or near) surfaces of the catalysts were assessed using XPS PEAK software (version of 4.1) through the deconvolution of peaks located at Fe 2p and S2p regime, respectively. While serving Shirley backgrounds, the peaks were fitted to a combination of Lorenzian and Gaussian curves at various binding energies. The amount of H_2O_2 decomposed during reactions was evaluated via 2,9-dimethyl-1,10-phenanthroline method using ultraviolet-visible spectrometer (Cary 100 UV–vis) at 454 nm according to the procedure reported by Kosaka and co-workers [32,33]. The amounts of leached Fe^{2+} species present in reaction mixtures were also measured via 1,10-phenanthroline method using Cary 100 UV–vis at 510 nm reported elsewhere [10,24]. Prior to analyses using UV–vis, calibration curves for H_2O_2 and Fe^{2+} quantification were constructed using known amount of H_2O_2 and $(NH_4)_2Fe(SO_4)_2·6H_2O$, respectively. The amounts of leached Fe and S species present in reaction mixtures were quantified using atomic absorption spectrometer (ICS 3000, Thermo Fisher Scientific) and inductively coupled plasma-optical emission spectrometer (iCAP 6500 DUO, Thermo Fisher Scientific) post the construction of external calibration curves for Fe and S species.

Reaction performance was evaluated using high-performance liquid chromatography (LC-20A, Shimadzu) equipped with an automatic injector (SIL-20A), a pump (LC-20AT), and a photodiode array detector (SPD-15C). This allowed for the quantification of phenol via reverse phase chromatography method, during which ODS column (5 μm particle size, 4.6 × 150 mm, Agilent) at 210 nm was utilized to quantify residual phenol concentration at a specific reaction time, whereas a mixture of water/methanol (vol. %, 50/50) with a flow rate of 1.0 mL min^{-1} was employed as a mobile phase. After building an external calibration curve for phenol, conversion of phenol (X_{PHENOL}) was determined using Eq. (1), where $C_{PHENOL,0}$ and C_{PHENOL} indicate the initial phenol concentration and phenol concentration at a specific reaction time, respectively.

$$X_{PHENOL}(\%) = \frac{C_{PHENOL,0}\,(molL^{-1}) - C_{PHENOL}\,(molL^{-1})}{C_{PHENOL,0}\,(molL^{-1})} \times 100 \tag{1}$$

2.3. Synthesis of FeS$_2$ and Fe$_3$S$_4$/Fe$_7$S$_8$

FeS_2 and Fe_3S_4/Fe_7S_8 were hydrothermally synthesized according to the procedures reported elsewhere [24,34]. In a typical FeS_2 synthesis, synthetic mixture comprising of 20 mmol of $FeSO_4·7H_2O$, 20 mmol of $Na_2S_2O_3·5H_2O$, 20 mmol of S, and 60 mL deionized (D. I.) water was loaded inside 200 mL Teflon-acid digestion sleeve. Typically, Fe_3S_4/Fe_7S_8 synthesis was initiated by putting synthetic mixture comprising of 10 mmol of $FeSO_4·7H_2O$, 10 mmol of L-cysteine, and 80 mL D. I. water into 200 mL Teflon-acid digestion sleeve. These were stirred at 600 rpm for 30 min, placed in a stainless steel vessel, and heated at 200 °C for 24 h. After cooling to 25 °C, the resulting Fe sulfides were isolated using vacuum filtration, rinsed with D. I. water, ethanol, carbon disulfide, and dried at 80 °C overnight.

2.4. Electro-Fenton reactions

Reactions were performed according to a slightly modified procedure we reported previously [9,35]. In a typical reaction run (i.e., the 1st recycle run), 0.1 mmol of phenol, 0.2 mol of Na_2SO_4, and 100 mL of D. I. water were loaded inside a 150 mL beaker at 25 °C and stirred at 240 rpm for 10 min, which provided the transparent reaction solution with pH of 7 (± 0.2). Two graphite plates (Groupe Carbone Lorraine, grade 2124) served as electrodes. One was used as-received and employed as an anode, whereas the other was employed as a cathode post coating with Fe-bearing catalyst. To coat the catalyst onto the cathode surface prior to the reaction run, 0.2 g of the catalyst was first mixed with a binder (poly(acrylic acid)) to form slurry. The graphite plate (i.e., cathode) was then coated with the slurry with a coated area of 3 cm × 4 cm and dried at 110 °C overnight. After that, two graphite plates were positioned vertically with the gap of 3 cm inside the beaker and initiated the electro-Fenton reaction with an electrical input of 3 V and 11.4 (± 1.1) mA under stirring at 240 rpm. 1 mL of reaction aliquot was taken at pre-determined time interval, quenched with 1 μL of methanol, and filtered using 0.45 μm sized-PES syringe filter (Whatman®) for finally collecting the reaction solution proper to HPLC analysis. Post the reaction, the catalyst was recovered through vacuum filtration using a Whatman filter paper (Grade 5, pore size: 2.5 μm), washed with 300 mL of D. I. water and 100 mL of ethanol, and dried at 80 °C overnight. All reaction runs were replicated more than twice to ensure the reproducibility of the reaction performance and to collect the catalyst enough for the next recycle run. H_2O_2 decomposition runs were conducted identically to the typical reaction run except phenol was replaced by 0.5 mmol of H_2O_2 in the absence of electrical input. In a typical filtration run, the catalyst was removed from the reaction mixture after 60 min by filtering the reaction mixture over Celite®545 (~20 g). Afterwards, the collected reaction mixture was further monitored.
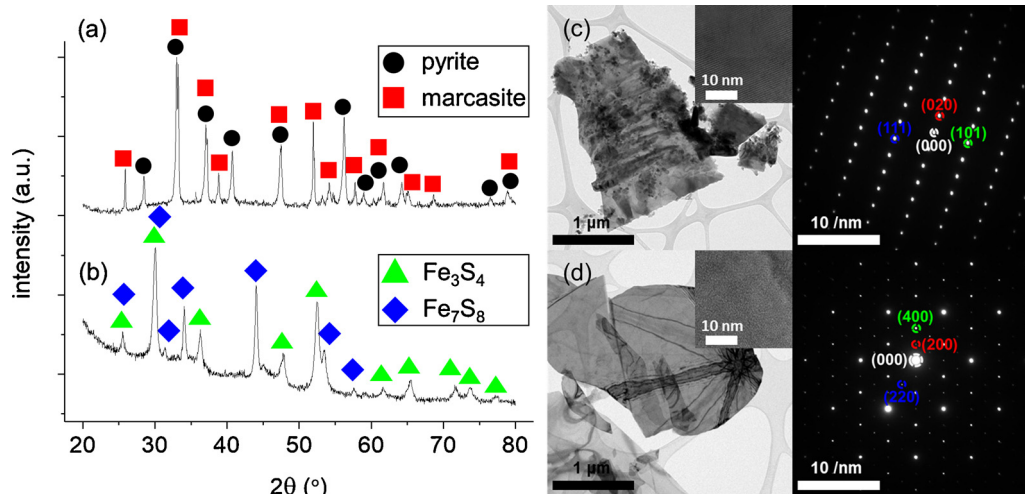
Fig. 2. XRD patterns for (a) FeS_2 and (b) Fe_3S_4/Fe_7S_8. HRTEM images and corresponding SAED patterns for (c) FeS_2 and (d) Fe_3S_4/Fe_7S_8. Spots with colored, dotted circles shown in the SAED patterns denote crystal planes of (c) marcasite and (d) pyrrhotite for FeS_2 and Fe_3S_4/Fe_7S_8, respectively.

3. Results and discussion

3.1. Catalyst synthesis and characterizations

FeS_2 and Fe_3S_4 were hydrothermally synthesized following the procedures delineated in Experimental section. In the case of FeS_2, hydrothermal synthetic procedure detailed elsewhere could not only provide pyrite but they also gave atomic S aggregates [36,37]. This was evidenced by the resulting materials' X-ray diffraction (XRD) patterns (not shown). Therefore, we followed alternative synthetic method [24,38], which solely produced FeS_2 with mixed bulk phases assigning as cubic pyrite (JCPDF No. of 00-024-0076) and orthorhombic marcasite (JCPDF No. of 01-089-2089), as shown in Fig. 2(a).

In the case of Fe_3S_4, aside from revealing bulk phase of cubic Fe_3S_4 (JCPDF No. of 01-089-1998), the resulting material also included crystal planes, which were in close agreement with those simulated for hexagonal Fe_7S_8 (JCPDF No: 00-024-0220 in Fig. 2(b)). This was ascribed to diverse Fe sulfide phases with the molar ratios of S to (Fe + S) as 0.5–0.66, all of which were present in binary Fe-S phase diagram (e.g., FeS, Fe_3S_4, Fe_7S_8, Fe_9S_{10}, $Fe_{10}S_{11}$, and $Fe_{11}S_{12}$) [29,39]. We therefore denoted this material as Fe_3S_4/Fe_7S_8. For the microscopic morphological observation of these materials, high resolution transmission electron microscope (HRTEM) analysis was conducted. Both sulfides exhibited rectangle-shaped conglomerates with the size of ~hundreds nm, as given in their HRTEM images (Fig. 2(c) and (d)). Selected area electron diffraction (SAED) patterns of both materials were also investigated to identify dominant crystal planes present in (or near) surface of the particulates. FeS_2 showed marcasite-rich surface, whereas Fe_3S_4/Fe_7S_8 showed pyrrhotite (Fe_7S_8)-rich surface. This suggested marcasite and pyrrhotite could mainly dissociate H_2O_2 during reaction runs, if these materials catalyzed the reaction heterogeneously. We also analyzed Fe-based oxides commercially available such as Fe_2O_3 and Fe_3O_4 for the comparison of their properties and reaction performance with those of FeS_2 and Fe_3S_4/Fe_7S_8. These materials showed typical rhombohedral Fe_2O_3 and cubic Fe_3O_4 crystal structures, as evidenced by their XRD patterns (Fig. S1(a)).

N_2 physisorption served to observe texture properties of all Fe-bearing materials, throughout which little porosities were consistent with no discernible trend, as quantified by Brunauer-Emmett-Teller (BET) surface area of ~$3\,m^2\,g^{-1}$ with Barrett–Joyner–Halenda (BJH) pore volume of ~$0.02\,cm^3\,g^{-1}$ (Table 1). CO is capable of binding with $Fe^{\delta+}/Fe^{3+}$ species via dipole-dipole interactions ($0 < \delta \le 2$) and was thus used as a probe molecule to quantify CO-accessible Lewis acid sites innate to the materials via CO-pulsed chemisorption [40–42]. Fe_2O_3

Table 1
Properties of Fe-bearing catalysts.

catalyst	S_{BET} [a] $(m^2\,g_{CAT}^{-1})$	V_{PORE} [a,b] $(cm^3\,g_{CAT}^{-1})$	N_{CO} [c] $(\mu mol\,g_{CAT}^{-1})$	k_{APP} [d] (X $10^{-3}\,min^{-1}$)
Fe_2O_3	4.7 ($\pm$0.1)	0.03	0.7	1.4 ($\pm$0.1)
Fe_3O_4	4.3 ($\pm$0.1)	0.02	0.4	2.6 ($\pm$0.1)
FeS_2	0.7 ($\pm$0.1)	0.01	0.3	8.0 ($\pm$0.3)
Fe_3S_4/Fe_7S_8	3.7 ($\pm$0.1)	0.01	0.4	11.5 ($\pm$0.7)

[a] via N_2 physisorption.
[b] via BJH.
[c] via CO-pulsed chemisorption.
[d] via pseudo-1st-order kinetic model.

provided larger amount of Lewis acid sites ($0.7\,\mu mol\,g_{CAT}^{-1}$) than Fe_3O_4 ($0.4\,\mu mol\,g_{CAT}^{-1}$), resulting from more abundant $Fe^{\delta+}/Fe^{3+}$ species inherent to Fe_2O_3 compared to Fe_3O_4. Unexpectedly, Fe sulfides revealed smaller quantity of CO-accessible sites than Fe oxide analogues ($\le 0.4\,\mu mol\,g_{CAT}^{-1}$) due in part to smaller electronegativity of S than O. This could render S-bound Fe species inherent to Fe sulfides to be less e^--deficient than those present in Fe oxides, which subsequently weakened the affinity of CO with surface-terminated Fe species present in Fe sulfides.

To further investigate surface character of the materials, their X-ray photoelectron (XP) spectroscopy analysis was performed. While revealing surface compositions nearly identical to their bulk stoichiometries (ratios of Fe/S as 0.4 ($\pm$0.1) for FeS_2; 0.7 ($\pm$0.2) for Fe_3S_4/Fe_7S_8), both FeS_2 and Fe_3S_4/Fe_7S_8 exhibited multiple states of surface Fe species (Fig. 3(a) and (b)). These were assigned as lattice Fe^{2+}, surface-exposed Fe^{2+}, O-bound Fe^{3+}, SO_3^{2-}-bound-Fe^{3+}, and SO_4^{2-}-bound Fe^{3+} species with binding energies centered at ~707, ~710, ~711, ~712, and ~714 eV in Fe 2p $_{3/2}$ spectra, respectively [24,43]. Notably, Fe_3S_4/Fe_7S_8 showed greater abundance of surface-terminated Fe^{2+} species than FeS_2 and thus could potentially outperform FeS_2 for dissociation of H_2O_2 to generate ·OH (Table 2). This could be further evidenced by S 2p regime of XP spectra for these materials (Fig. 3(c) and (d)), which showed Fe_3S_4/Fe_7S_8 consisted of larger portion of surface-exposed S_2^{2-} species than FeS_2 (Table 2). For comparison, surface feature of two Fe oxides was also investigated using their XP spectra at Fe 2p regime. The spectra showed Fe_3O_4 provided larger abundance of surface $Fe^{\delta+}$ ($0 < \delta \le 2$) species (~46%) than Fe_2O_3 (~41%) and thus could potentially provide enhanced ·OH evolution performance compared to Fe_2O_3 (Fig. S1(b) and (c)).
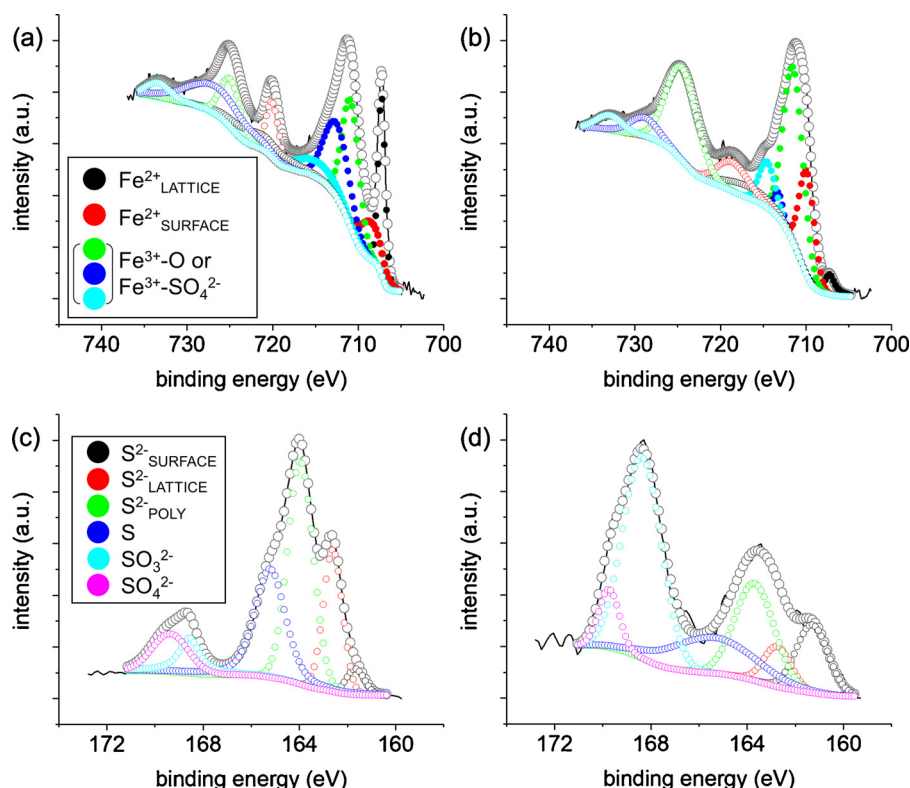
Fig. 3. Fe 2p and S 2p regions of XP spectra for FeS$_2$ and Fe$_3$S$_4$/Fe$_7$S$_8$ prior to the 1st recycle runs: (a) Fe 2p for FeS$_2$, (b) Fe 2p for Fe$_3$S$_4$/Fe$_7$S$_8$, (c) S 2p for FeS$_2$, and (d) S 2p for Fe$_3$S$_4$/Fe$_7$S$_8$. In (a) and (b), solid and empty symbols indicate surface Fe species located at Fe 2p$_{3/2}$ and Fe 2p$_{1/2}$, respectively. Black lines indicate raw XP spectra, whereas grey-colored, empty circle indicate fitted XP spectra.

Table 2
Relative abundance of surface (SURF) Fe^{2+}, S^{2-} species, and molar ratio of Fe to S present on/near surfaces (Fe/S) for FeS$_2$ and Fe$_3$S$_4$/Fe$_7$S$_8$.[a]

	material	Fe$^{2+}_{SURF}$	S$^{2-}_{SURF}$	Fe/S
before the 1st run	FeS$_2$	12.0	3.0	0.4 ($\pm$ 0.1)
	Fe$_3$S$_4$/Fe$_7$S$_8$	24.7	11.4	0.7 ($\pm$ 0.2)
post the 3rd run	FeS$_2$	35.7	6.7	0.8 ($\pm$ 0.1)
	Fe$_3$S$_4$/Fe$_7$S$_8$	34.0	17.4	1.2 ($\pm$ 0.1)

[a] quantified using spectra at Fe 2p $_{3/2}$ and S 2p regimes (see Tables S1 and S2; Figs. 3 and S6).

3.2. Reactions

3.2.1. Phenol decomposition performance on Fe-bearing catalysts

We then performed electro-Fenton-assisted phenol degradation experiments using the Fe-bearing materials as catalysts. Again, the target of these reaction runs was to validate our two major hypotheses as to whether 1) Fe sulfides can outperform Fe oxides to decompose phenol via enhanced ·OH productivity and 2) Fe sulfides can proceed the reactions via heterogeneous manner. To corroborate these hypotheses, the catalyst was coated onto the cathode surface prior to the electro-Fenton runs to accomplish instantaneous/promoted contact of catalytic surface with H$_2$O$_2$ evolved through O$_2$ reduction (Fig. 1(c)). This was anticipated to attain greater ·OH productivity primarily through heterogeneous reactions, as depicted in Fig. 1(f) and (g). In addition, pH values were monitored throughout all reaction runs and detected as 7 ($\pm$ 0.2) prior to the reactions and as 5 ($\pm$ 0.3) post the reactions. This was in contrast to the reactions by E. Brillas and co-workers, during which pH values were auto-adjusted to ~3 in the middle of the reaction [22]. This could result from far larger electrical powers exerted during their reactions (~3 W) than those in our runs ($\leq$0.04 W). This was because such great powers could spur two side-reactions, wherein Fe^{2+}/Fe^{3+} species were leached from Fe sulfides while releasing H$^+$ species, as illustrated in Fig. 1(d) and (e). Relatively neutral pH

conditions in our reaction runs was expected to reduce undesired Fe leaching, thus potentially proceeding the phenol degradation mainly through heterogeneous catalytic ·OH evolution.

Phenol decomposition activities for all catalysts were evaluated by their initial phenol consumption rates, which were obtained through the multiplication of apparent reaction rate constants (k_{APP}) with initial phenol concentration (C$_{PHENOL, 0}$) [35,44]. k_{app} values were determined through fitting of reaction data to pseudo-1st-order kinetic model (Fig. S2 and Table 1) [35,44]. For the comparison of H$_2$O$_2$ scission activities among O or S-modified Fe sites incorporated into the catalysts, the initial reaction rates were normalized with respect to the gram of catalyst or the amount of CO-accessible sites (N_{CO}) used during the reactions. This provided two distinct values of $-$r$_{INITIAL, g CAT}$ or $-$r$_{INITIAL, NCO}$, respectively (Fig. 4). Expected by our previous findings via XP spectroscopy, Fe$_3$O$_4$ showed larger $-$r$_{INITIAL, g CAT}$ than Fe$_2$O$_3$, which resulted from greater amount of Fe^{2+} inherent to Fe$_3$O$_4$ than Fe$_2$O$_3$. As previously stated, Fe$_2$O$_3$ had a larger quantity of CO-accessible sites including both Fe^{3+} and Fe$^{\delta+}$ species compared to Fe$_3$O$_4$. The surface of Fe$_2$O$_3$, however, was inferred to be mainly populated with Fe^{3+} species rather than Fe^{2+} species, thereby providing smaller -r$_{INITIAL}$ value post normalization on N$_{CO}$ than Fe$_3$O$_4$.

Aside from substantially increasing phenol conversions (X$_{PHENOL}$ of ~40% for oxides; ~100% for sulfides after 8 h), $-$r$_{INITIAL, g CAT}$ values were considerably enhanced when Fe sulfides were used as catalysts. Of importance, N$_{CO}$ of Fe$_3$O$_4$ was almost identical to that of Fe$_3$S$_4$/Fe$_7$S$_8$ as ~0.4 μmol$_{CO}$ g$_{CAT}^{-1}$. This highly suggested S-modified Fe^{2+} species present in Fe sulfides outperformed O-modified Fe^{2+} analogue present in Fe oxides for the production of ·OH used to fragment phenol. This was further corroborated by the values of $-$r$_{INITIAL, NCO}$ for these catalysts, which showed there are ~5 fold increase in $-$r$_{INITIAL, NCO}$ value after changing the type of catalyst from Fe$_3$O$_4$ to Fe$_3$S$_4$/Fe$_7$S$_8$. Of additional importance, Fe$_3$S$_4$/Fe$_7$S$_8$ further promoted ·OH production in comparison with FeS$_2$, as evidenced by greater -r$_{INITIAL, g CAT}$ of Fe$_3$S$_4$/Fe$_7$S$_8$, which was again caused by larger N$_{CO}$ innate to Fe$_3$S$_4$/Fe$_7$S$_8$ than FeS$_2$. In addition, phenol decomposition run on Fe$_3$S$_4$/Fe$_7$S$_8$ catalyst was also performed with the use of strong ·OH scavenger, *tert*-butyl
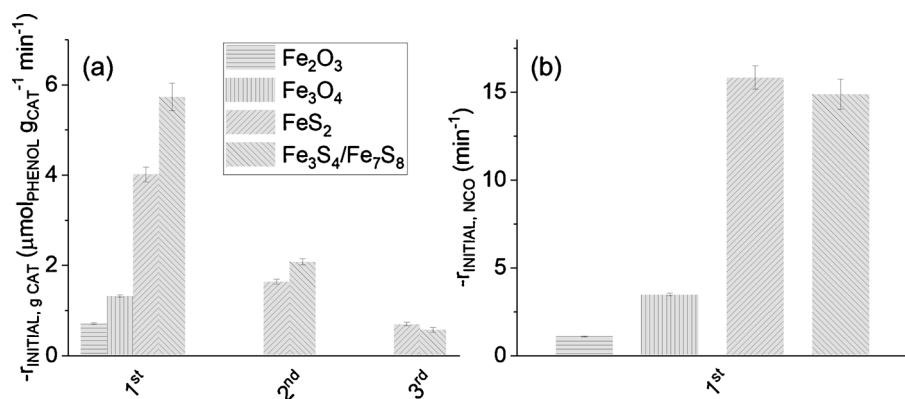
Fig. 4. Initial phenol decomposition reaction rates normalized with respect to the amount of catalyst ($-r_{INITIAL, \, g \, CAT}$) or the amount of CO-accessible sites ($-r_{INITIAL, \, NCO}$) for Fe-bearing catalysts: (a) Values of $-r_{INITIAL, \, g \, CAT}$ determined throughout multiple recycle runs and (b) Values of $-r_{INITIAL, \, NCO}$ obtained during the 1st recycle runs. Reaction condition: 0.2 g of catalyst; 0.1 mmol of phenol; 0.2 mol of Na_2SO_4; 100 mL of deionized water; 25 °C; 3 V; 11.4 (± 1.1) mA; 240 rpm.

alcohol [45,46]. The purpose of this control experiment was to substantiate that the degradation of phenol was mainly controlled by ·OH species evolved via catalytic H_2O_2 scission. Interestingly, even with the addition of *tert*-butyl alcohol during the reaction, ∼45% of phenol was still converted after 8 h (Fig. S3). This could result from continuous generation of H_2O_2 via cathodic O_2 reduction and anodic oxidation during electro-Fenton reaction [22,47], wherein the amount of H_2O_2- derived ·OH species could exceed that of *tert*-butyl alcohol. However, phenol decomposition efficiency in the control run was reduced markedly, when comparing with the counterpart run (i.e., without *tert*-butyl alcohol), which showed the phenol conversion of ∼100% after 8 h. This provided evidence that ·OH produced via H_2O_2 cleavage on iron sulfide was the major active source to degrade phenol. All of the reaction runs discussed in this section could demonstrate that greater ·OH production performance was attained through the alteration of catalyst type from Fe oxides to Fe sulfides, among which Fe_3S_4/Fe_7S_8 outperformed FeS_2.

3.2.2. H_2O_2 decomposition performance on Fe sulfide catalysts

It was reported in literatures that greater H_2O_2 decomposition performance of a catalyst could validate its ability to produce greater amount of ·OH species during Fenton reactions [48–50]. Hence, we performed control reaction runs using Fe sulfide catalysts under an identical condition to that employed during the normal phenol decomposition run except H_2O_2 was added in the absence of both phenol and electrical power input (Fig. 5 and S4). The objective of this study was to further verify if Fe_3S_4/Fe_7S_8 with greater N_{CO} could enhance H_2O_2 dissociation performance over FeS_2. In addition to exhibiting

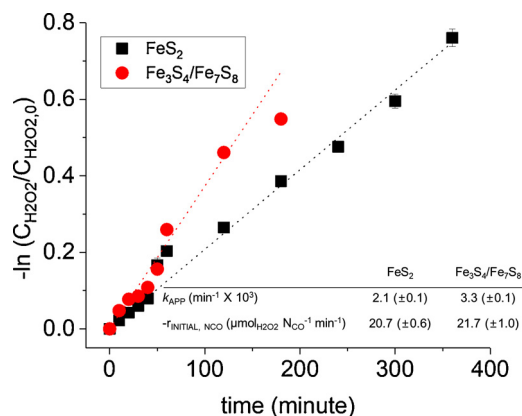**Fig. 5.** H_2O_2 decomposition experiments using FeS_2 and Fe_3S_4/Fe_7S_8. Reaction data is fitted to pseudo-1st-order kinetic model (dotted lines) with regression factors of ≥ 0.96. $C_{H2O2,0}$ denotes initial H_2O_2 concentration, whereas C_{H2O2} denotes H_2O_2 concentration at a specific reaction time. Reaction condition: 0.2 g of catalyst; 0.5 mmol of H_2O_2; 0.2 mol of Na_2SO_4; 100 mL of deionized water; 25 °C; 240 rpm.

greater H_2O_2 conversion (∼80% for Fe_3S_4/Fe_7S_8; ∼65% for FeS_2 after 8 h), Fe_3S_4/Fe_7S_8 also promoted initial H_2O_2 consumption rate per unit gram of catalyst by almost ∼2 fold. (∼9 $\mu mol_{H2O2} \, g_{CAT}^{-1} \, min^{-1}$ for Fe_3S_4/Fe_7S_8; ∼5 $\mu mol_{H2O2} \, g_{CAT}^{-1} \, min^{-1}$ for FeS_2). Most importantly, values of either initial phenol consumption rate or initial H_2O_2 decomposition rate for these sulfide catalysts were very similar post N_{CO} normalization (Figs. 4b and 5). Obviously, these experimental results validated the following claim that both sulfide catalysts can catalyze ·OH production-directed phenol decomposition mainly using S-modified Fe^{2+} species.

3.2.3. Recycle runs to decompose phenol on Fe sulfide catalysts

The nature of Fe sulfides to heterogeneously catalyze ·OH production was demonstrated by a series of recycle phenol decomposition runs, throughout which 1) XRD patterns, 2) XP spectra of these catalysts, and 3) the amount of homogeneous Fe^{2+} or total Fe/S species leached from the catalysts were also monitored. The Fe sulfides showed continuous reduction of $-r_{INITIAL, \, g \, CAT}$ values during each of the subsequent recycle runs, declining from ∼4 to ∼1 $\mu mol_{PHENOL} \, g_{CAT}^{-1} \, min^{-1}$ for FeS_2, whereas declining from ∼6 to ∼1 $\mu mol_{PHENOL} \, g_{CAT}^{-1} \, min^{-1}$ for Fe_3S_4/Fe_7S_8 (Fig. 4(a)). Bulk sulfide phases of these catalysts were retained post the 3rd recycle run (Fig. S5). Hence, structural deformation of Fe sulfides or their transition to oxide analogues should not be responsible for the decrease in $-r_{INITIAL, \, g \, CAT}$ values during the multiple runs. XP spectra of these catalyst post the 3rd recycle run also showed surface-terminated Fe^{2+} and S^{2-} species were still present, which was in line with the XRD analysis for these catalysts discussed above. (Fig. S6 and Table 2).

The amounts of Fe^{2+} species leached from the sulfides' surfaces, however, were consistent as 0.3 (± 0.1) mol. % Fe throughout the recycle runs. This suggested that leached Fe^{2+} were minor homogeneous species to catalyse H_2O_2 scission. This was because one should have observed the persistent values of $-r_{INITIAL, \, g \, CAT}$ during each of the multiple runs, if ·OH production were mainly driven by homogeneous Fe^{2+} species. It should be noted that total Fe and S species leaving FeS_2 or Fe_3S_4/Fe_7S_8 surfaces during multiple runs included homogeneous species as well as heterogeneous, unsupported species that were weakly bound to the surfaces prior to reaction runs. Apparently, both sulfides were composed of hundreds nm-sized rectangles (Fig. 2(c) and (d)), which could readily pass through filters during the recycle runs. In the case of FeS_2, total amount of leached Fe and S species showed increasing trend throughout recycle runs (∼5.5 → ∼7.9 mol. % for Fe; ∼4.7 → ∼8.8 mol. % for S). However, the trend of $-r_{INITIAL, \, g \, CAT}$ for FeS_2 was counter-current to its trend of total quantities of leached Fe and S species during each of multiple recycle run. This leaded to the feasible conclusion that catalytic ·OH production on FeS_2 was mainly controlled by heterogeneous, supported surface Fe^{2+} species.

In contrast to FeS_2, Fe_3S_4/Fe_7S_8 showed con-current trends for $-r_{INITIAL, \, g \, CAT}$ and leached Fe and S quantities (∼5.7 → ∼0.3 mol. % for Fe; ∼8.0 → ∼2.5 mol. % for S), both of which were steadily
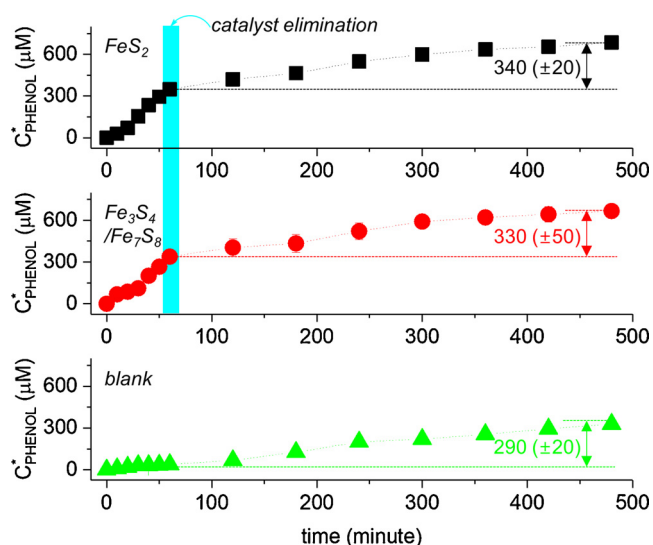
Fig. 6. Reaction profiles (amount of phenol consumed (C^*_{PHENOL}) versus time) obtained during filtration experiments using FeS_2, Fe_3S_4/Fe_7S_8, and blank. In the blank experiment, no catalyst was coated on the cathode prior to the reaction run. Reaction condition: 0.2 g (or 0 g) of catalyst; 0.1 mmol of phenol; 0.2 mol of Na_2SO_4; 100 mL of deionized water; 25 °C; 3 V; 11.4 (± 1.1) mA; 240 rpm.

reduced up to the 3rd recycle run. Unexpectedly, XP spectra of FeS_2 and Fe_3S_4/Fe_7S_8 post the 3rd run showed such interesting trend that relative abundances of surface Fe^{2+}/S^{2-} species were even increased in comparison with those prior to the 1st run (Table 2). If this was the case, one expected to observe the increase in $-r_{INITIAL, \ g \ CAT}$ values throughout the recycle runs for both catalysts.

3.2.4. Filtration runs to decompose phenol on Fe sulfide catalysts

Albeit the recycle runs on FeS_2 could provide partial evidence to catalyze H_2O_2 decomposition heterogeneously, the recycle runs on Fe_3S_4/Fe_7S_8 provided the results which were contradictable to our hypothesis of heterogeneous catalyzed H_2O_2 dissociation on Fe_3S_4/Fe_7S_8. To better understand the phenomena that occured on the surfaces of Fe sulfide catalysts during the reaction runs (Fe_3S_4/Fe_7S_8, in particular), we thus performed filtration study during the phenol decomposition (Fig. 6). This experiment was designed for the observation of phenol decomposition performance mainly contributed by homogeneous, leached Fe^{2+} and S^{2-} species along with their amounts in the middle of the reaction runs. We expected this experiment could clarify whether Fe_3S_4/Fe_7S_8 performed the reaction heterogeneously and what the roles of leached S^{2-} was to promote H_2O_2 scission. For this experiment, a catalyst-coated cathode was exchanged to a catalyst-uncoated, fresh cathode after an hour, whereas a reaction mixture were filtered simultaneously. Afterward, the collected reaction mixture with the fresh cathode were used to further monitor the reaction performance. Even after an hour, we could see unceasing consumption of phenol up to the 8 h, where FeS_2 and Fe_3S_4/Fe_7S_8 showed similar quantities of phenol consumption as 340 (± 20) μmole and 330 (± 50) μmole, respectively (Fig. 6). These quantities, however, were comparable to the amount of phenol consumed on a blank experiment using catalyst-uncoated, bare cathode during an identical period of reaction (i.e., 290 (± 20) μmole of phenol from 1 to 8 h). This could result from the anodic oxidation on the graphite electrode, leading to the generation of ·OH used to decompose phenol (Fig. 1(j)) [22,47]. Apparently, this experiment provided evidence that surface-exposed, heterogeneous Fe^{2+} species deposited on Fe sulfides primarily directed the catalytic · OH production and the subsequent phenol degradation.

The quantities of Fe and S species present in reaction mixtures post filtration (denoted as filtration run) were also analyzed and compared

with those post the 1st run, where no filtration procedure in the middle of the reaction was involved (normal run). Fe sulfides showed smaller Fe leaching post filtration run than that post the normal run (~ 1.8 mol. % Fe for FeS_2; ~ 1.2 mol. % Fe for Fe_3S_4/Fe_7S_8). This was caused by less exposure of Fe sulfides to O_2 and H_2O_2 prior to the filtration in the filtration run, thereby generating smaller quantity of homogeneous Fe species via Fig. 1(d) and (e) than the normal run.

In contrast, Fe sulfides provided larger S leaching post filtration run than that post the normal run (~ 11.4 mol. % S for FeS_2; ~ 9.7 mol. % S for Fe_3S_4/Fe_7S_8). The substantial S leaching up to an hour of the reaction run was highly likely, as given in a previous study by D. Wu and co-workers showing the similar phenomenon on FeS_2 during Fenton reaction [23]. In addition, considerable S leaching could be accumulated up to the 3rd recycle run, leading to the increase in the surface ratios of Fe to S for the sulfide catalysts post the 3rd runs in comparison with those prior to the 1st run (Table 2). The S leaching was reported to play multiple roles such as the direct formation of ·OH and the acceleration of homogeneous Fe^{2+}/Fe^{3+} redox cycle, both of which aided in producing greater ·OH species via homogeneous catalysis [23]. The filtration run that decomposed phenol almost identically to the blank run during the identical period of reaction run (1 h–8 h), again, corroborated that these two roles of leached S species were insignificant to evolve ·OH. Based on the previous study by Wu and co-workers [23], it was speculated that some of leached S species (S^{2-}) could help reconstruct surface with Fe sulfide feature through the combination of S^{2-} with leached, homogeneous Fe^{2+} species. Indeed, this claim could be verified by the increase in surface abundance for surface-terminated, unleached Fe^{2+} and S^{2-} species post the 3rd reaction compared to that prior to the 1st run when comparing XP spectra of Fe sulfides obtained post the multiple runs (Table 2).

In spite of having promoted abundance of unleached surface Fe^{2+} species beneficial to ·OH production during each of recycle runs to degrade phenol, the catalysts could not increase $-r_{INITIAL, \ g \ CAT}$. Apparently, catalyst particles on the cathode were subjected to continuous exposure to mechanical stirring and dynamic surface reactions involving the generation/consumption of highly active species throughout the recycle runs. This could weaken affinity among particles, render them vulnerable to detach from aggregated particulates, and reduce the likelihood for the resulting detached particles to instantaneously/vigorously interact with H_2O_2 species generated on the cathode.

4. Conclusions

To sum up, this study has verified two hypothetical benefits expected by the use of Fe_3S_4/Fe_7S_8 as electro-Fenton catalyst to decompose phenol through detailed characterizations combined with kinetic assessments.

As per the 1st advantage, S-modified, surface-terminated Fe^{2+} species outperformed O-modified, surface-exposed Fe^{2+} species for producing ·OH, as evidenced by greater mass-normalized initial reaction rates of Fe sulfides than those of Fe oxides in the phenol decomposition. In addition, Fe_3S_4/Fe_7S_8 provided increased quantity of surface Fe^{2+} species active to dissociate H_2O_2 in comparison with those of FeS_2. This was demonstrated by the properties of Fe_3S_4/Fe_7S_8 superior to FeS_2 such as larger amount of CO-accessible sites and increased mass-normalized initial reaction rates to decompose phenol or to dissociate H_2O_2. Noteworthy, similarity of CO-normalized initial reaction rates between FeS_2 and Fe_3S_4/Fe_7S_8 in both reactions provided evidence that surface-exposed Fe^{2+} species present in Fe sulfides were the major source to catalyze ·OH production.

As per the 2nd advantage, it was evident that Fe sulfides could catalyze ·OH production heterogeneously under mild, near-neutral environments. This was evidenced by a series of recycle phenol degradation runs. Constant amount of homogeneous Fe^{2+} species leached from the sulfide catalysts during each of multiple runs were discrepant

to the trend of mass-normalized initial reaction rates with continuous reduction. Filtration experiments during the phenol decomposition also supported the catalytic nature of Fe sulfides to heterogeneously facilitate ·OH evolution. This was because the quantity of phenol consumed post filtration (i.e., removal of catalyst from the reaction mixture) was almost same to that observed in blank reaction (i.e., no catalyst employed) during the identical period of reaction run. In conjunction with XP spectroscopy analyses, this also demonstrated the role of leached S species during the reactions such that leached S species could bind with leached Fe species and rebuild the surface with Fe sulfide character rather than homogeneously catalyzing ·OH generation.

Although this study showcased concrete evidence associated with heterogeneous catalytic nature of Fe_3S_4/Fe_7S_8 to efficiently produce ·OH species, the decrease in phenol degradation performance throughout the recycle runs opens additional task that is related with the reaction longevity. We currently speculate the type of binder used to immobilize the catalyst onto the cathode is another factor to consider for realizing substantial longevity to degrade phenol and this is our ongoing research.

Contributor

Y. J. Choe performed experiments and contributed partially to writing the draft. Dr. J. Y. Byun helped set the research direction up and provided comments on the materials' properties. Dr. S. H. Kim helped set the research direction up, aided in characterizing the materials' properties, and provided comments on the draft. Dr. J. Kim performed experiments, characterized materials' properties/reaction performance, and wrote up the draft. All authors declared that the contents written in the draft are true and approved the submission of the draft to Appl. Catal. B.

Acknowledgements

Appendix A. Supplementary data

Supplementary material related to this article can be found, in the online version, at doi:https://doi.org/10.1016/j.apcatb.2018.03.110.

References

[1] A.D. Bokare, W. Choi, Review of iron-free Fenton-like systems for activating H_2O_2 in advanced oxidation processes, J. Hazard. Mater. 275 (2014) 121–135.

[2] E. Brillas, I. Sirés, M.A. Oturan, Electro-Fenton process and related electrochemical technologies based on Fenton's reaction chemistry, Chem. Rev. 109 (2009) 6570–6631.

[3] C.K. Duesterberg, W.J. Cooper, T.D. Waite, Fenton-mediated oxidation in the presence and absence of oxygen, Environ. Sci. Technol. 39 (2005) 5052–5058.

[4] M. Antonopoulou, E. Evgenidou, D. Lambropoulou, I. Konstantinou, A review on advanced oxidation processes for the removal of taste and odor compounds from aqueous media, Water Res. 53 (2014) 215–234.

[5] F.C. Moreira, R.A.R. Boaventura, E. Brillas, V.J.P. Vilar, Electrochemical advanced oxidation processes: a review on their application to synthetic and real wastewaters, Appl. Catal. B 202 (2017) 217–261.

[6] H. Li, J. Shang, Z. Yang, W. Shen, Z. Ai, L. Zhang, Oxygen vacancy associated surface Fenton chemistry: surface structure dependent hydroxyl radicals generation and substrate dependent reactivity, Environ. Sci. Technol. 51 (2017) 5685–5694.

[7] P.V. Nidheesh, Heterogeneous Fenton catalysts for the abatement of organic pollutants from aqueous solution: a review, RSC Adv. 5 (2015) 40552–40577.

[8] Y. Yang, T. Chen, M. Sumona, B.S. Gupta, Y. Sun, Z. Hu, X. Zhan, Utilization of iron sulfides for wastewater treatment: a critical review, Rev. Environ. Sci. Biotechnol. 16 (2017) 289–308.

[9] T.M. Do, J.Y. Byun, S.H. Kim, An electro-Fenton system using magnetite coated metallic foams as cathode for dye degradation, Catal. Today 295 (2017) 48–55.

[10] J. Du, J. Bao, X. Fu, C. Lu, S.H. Kim, Mesoporous sulfur-modified iron oxide as an effective Fenton-like catalyst for degradation of bisphenol A, Appl. Catal. B 184 (2016) 132–141.

[11] T.M. Do, J.Y. Byun, S.H. Kim, Magnetite-coated metal foams as one-body catalysts for Fenton-like reactions, Res. Chem. Intermed. 43 (2017) 3481–3492.

[12] I. Velo-Gala, J.J. López-Peñalver, M. Sánchez-Polo, J. Rivera-Utrilla, Comparative study of oxidative degradation of sodium diatrizoate in aqueous solution by H_2O_2/Fe^{2+}, H_2O_2/Fe^{3+}, Fe (VI) and UV, H_2O_2/UV, $K_2S_2O_8/UV$, Chem. Eng. J. 241 (2014) 504–512.

[13] S. Bae, D. Kim, W. Lee, Degradation of diclofenac by pyrite catalyzed Fenton oxidation, Appl. Catal. B 134 (2013) 93–102.

[14] D. Rickard, G.W. Luther, Chemistry of iron sulfides, Chem. Rev. 107 (2007) 514–562.

[15] Y. Gong, J. Tang, D. Zhao, Application of iron sulfide particles for groundwater and soil remediation: a review, Water Res. 89 (2016) 309–320.

[16] M. Arienzo, Oxidizing 2,4,6-trinitrotoluene with pyrite-H_2O_2 suspensions, Chemosphere 39 (1999) 1629–1638.

[17] H. Che, S. Bae, W. Lee, Degradation of trichloroethylene by Fenton reaction in pyrite suspension, J. Hazard. Mater. 185 (2011) 1355–1361.

[18] K. Choi, S. Bae, W. Lee, Degradation of pyrene in cetylpyridinium chloride-aided soil washing wastewater by pyrite Fenton reaction, Chem. Eng. J. 249 (2014) 34–41.

[19] L.Od.B. Benetoli, B.M. Cadorin, V.Z. Baldissarelli, R. Geremias, I.G. de Souza, N.A. Debacher, Pyrite-enhanced methylene blue degradation in non-thermal plasma water treatment reactor, J. Hazard. Mater. 237–238 (2012) 55–62.

[20] E.-J. Kim, J.-H. Kim, A.-M. Azad, Y.-S. Chang, Facile synthesis and characterization of Fe/FeS nanoparticles for environmental applications, ACS Appl. Mater. Interfaces 3 (2011) 1457–1462.

[21] F. Hao, W. Guo, X. Lin, Y. Leng, A. Wang, X. Yue, L. Yan, Degradation of acid orange 7 in aqueous solution by dioxygen activation in a pyrite/H_2O/O_2 system, Environ. Sci. Pollut. Res. 21 (2014) 6723–6728.

[22] S. Ammar, M.A. Oturan, L. Labiadh, A. Guersalli, R. Abdelhedi, N. Oturan, E. Brillas, Degradation of tyrosol by a novel electro-Fenton process using pyrite as heterogeneous source of iron catalyst, Water Res. 74 (2015) 77–87.

[23] L. Zhao, Y. Chen, Y. Liu, C. Luo, D. Wu, Enhanced degradation of chloramphenicol at alkaline conditions by S(-II) assisted heterogeneous Fenton-like reactions using pyrite, Chemosphere 188 (2017) 557–566.

[24] W. Li, Y. Wang, Z. Ai, L. Zhang, Hydrothermal synthesis of FeS2 as a high-efficiency Fenton reagent to degrade alachlor via superoxide-mediated Fe(II)/Fe(III) cycle, ACS Appl. Mater. Interfaces 7 (2015) 28534–28544.

[25] L. Guo, F. Chen, X. Fan, W. Cai, J. Zhang, S-Doped α-Fe_2O_3 as a highly active heterogeneous Fenton-like catalyst towards the degradation of acid orange 7 and phenol, Appl. Catal. B 96 (2010) 162–168.

[26] L. Chang, A.P. Roberts, Y. Tang, B.D. Rainford, A.R. Muxworthy, Q. Chen, Fundamental magnetic parameters from pure synthetic greigite (Fe_3S_4), J. Geophys. Res. 113 (2008) B06104.

[27] L. Chang, B.D. Rainford, J.R. Stewart, C. Ritter, A.P. Roberts, Y. Tang, Q. Chen, Magnetic structure of greigite (Fe_3S_4) probed by neutron powder diffraction and polarized neutron diffraction, J. Geophys. Res. 114 (2009) B07101.

[28] J. Chun, H. Lee, S.-H. Lee, S.-W. Hong, J. Lee, C. Lee, J. Lee, Magnetite/mesocellular carbon foam as a magnetically recoverable fenton catalyst for removal of phenol and arsenic, Chemosphere 89 (2012) 1230–1237.

[29] J.M. Soon, L.Y. Goh, K.P. Loh, Y.L. Foo, L. Ming, J. Ding, Highly textured, magnetic $Fe_{(1+x)}S$ nanorods grown on silicon, Appl. Phys. Lett. 91 (2007) 084105.

[30] L.G.C. Villegas, N. Mashhadi, M. Chen, D. Mukherjee, K.E. Taylor, N. Biswas, A short review of techniques for phenol removal from wastewater, Curr. Pollut. Rep. 2 (2016) 157–167.

[31] M.S. Ramos, J.L. Dávila, F. Esparza, F. Thalasso, J. Alba, A.L. Guerrero, F.J. Avelar, Treatment of wastewater containing high phenol concentrations using stabilisation ponds enriched with activated sludge, Water. Sci. Technol. 51 (2005) 257–260.

[32] K. Kosaka, H. Yamada, S. Matsui, S. Echigo, K. Shishida, Comparison among the methods for hydrogen peroxide measurements to evaluate advanced oxidation processes: application of a spectrophotometric method using copper(II) ion and 2,9-dimethyl-1,10-phenanthroline, Environ. Sci. Technol. 32 (1998) 3821–3824.

[33] A.N. Baga, G.R.A. Johnson, N.B. Nazhat, R.A. Saadalla-Nazhat, A simple spectrophotometric determination of hydrogen peroxide at low concentrations in aqueous solution, Anal. Chim. Acta 204 (1988) 349–353.

[34] F. Cao, W. Hu, L. Zhou, W. Shi, S. Song, Y. Lei, S. Wang, H. Zhang, 3D Fe_3S_4 flower-like microspheres: high-yield synthesis via a biomolecule-assisted solution approach, their electrical, magnetic and electrochemical hydrogen storage properties, Dalton Trans. (2009) 9246–9252.

[35] J. Kim, N.D. McNamara, J.C. Hicks, Catalytic activity and stability of carbon supported v oxides and carbides synthesized via pyrolysis of MIL-47 (V), Appl. Catal. A 517 (2016) 141–150.

[36] G. Kaur, B. Singh, P. Singh, M. Kaur, K.K. Buttar, K. Singh, A. Thakur, R. Bala, M. Kumar, A. Kumar, Preferentially grown nanostructured iron disulfide (FeS_2) for removal of industrial pollutants, RSC Adv. 6 (2016) 99120–99128.

[37] A. Akhoondi, M. Aghaziarati, N. Khandan, Production of highly pure iron disulfide nanoparticles using hydrothermal synthesis method, Appl. Nanosci. 3 (2013) 417–422.

[38] R. Wu, Y.F. Zheng, X.G. Zhang, Y.F. Sun, J.B. Xu, J.K. Jian, Hydrothermal synthesis and crystal structure of pyrite, J. Cryst. Growth 266 (2004) 523–527.

[39] M. Akhtar, M.A. Malik, F. Tuna, P. O'Brien, The synthesis of iron sulfide nanocrystals from tris(O-alkylxanthato)iron(iii) complexes, J. Mater. Chem. A 1 (2013) 8766–8774.

[40] J. Kim, D.B. Go, J.C. Hicks, Synergistic effects of plasma-catalyst interactions for CH_4 activation, Phys. Chem. Chem. Phys. 19 (2017) 13010–13021.

[41] D.J. Rensel, J. Kim, V. Jain, Y. Bonita, N. Rai, J.C. Hicks, Composition-directed Fe$_x$Mo$_{2-x}$P bimetallic catalysts for hydrodeoxygenation reactions, Catal. Sci. Technol. 7 (2017) 1857–1867.

[42] J. Kim, M.S. Abbott, D.B. Go, J.C. Hicks, Enhancing C–H bond activation of methane via temperature-controlled, catalyst–plasma interactions, ACS Energy Lett. 1 (2016) 94–99.

[43] W. Han, M. Gao, Investigations on iron sulfide nanosheets prepared via a single-source precursor approach, Cryst. Growth Des. 8 (2008) 1023–1030.

[44] J. Kim, N.D. McNamara, T.H. Her, J.C. Hicks, Carbothermal reduction of Ti-Modified IRMOF-3: an adaptable synthetic method to support catalytic nano-particles on carbon, ACS Appl. Mater. Interfaces 5 (2013) 11479–11487.

[45] P. Liu, C. Li, Z. Zhao, G. Lu, H. Cui, W. Zhang, Induced effects of advanced oxidation processes, Sci. Rep. 4 (2014) 4018.

[46] X.-R. Xu, Z.-Y. Zhao, X.-Y. Li, J.-D. Gu, Chemical oxidative degradation of methyl *tert*-butyl ether in aqueous solution by Fenton's reagent, Chemosphere 55 (2004) 73–79.

[47] E. Rosales, M. Pazos, M.A. Sanromán, Advances in the electro-fenton process for remediation of recalcitrant organic compounds, Chem. Eng. Technol. 35 (2012) 609–617.

[48] J. He, W. Ma, J. He, J. Zhao, J.C. Yu, Photooxidation of azo dye in aqueous dispersions of H$_2$O$_2$/α-FeOOH, Appl. Catal. B 39 (2002) 211–220.

[49] M. Cheng, W. Ma, J. Li, Y. Huang, J. Zhao, Yx. Wen, Y. Xu, Visible-light-assisted degradation of dye pollutants over Fe(III)-loaded resin in the presence of H$_2$O$_2$ at neutral pH values, Environ. Sci. Technol. 38 (2004) 1569–1575.

[50] R.C.C. Costa, M.F.F. Lelis, L.C.A. Oliveira, J.D. Fabris, J.D. Ardisson, R.R.V.A. Rios, C.N. Silva, R.M. Lago, Novel active heterogeneous Fenton system based on Fe$_{3-x}$M$_x$O$_4$ (Fe, Co, Mn, Ni): the role of M^{2+} species on the reactivity towards H$_2$O$_2$ reactions, J. Hazard. Mater. 129 (2006) 171–178.